Elucidating Contributions of Anthropogenic Volatile Organic Compounds and Particulate Matter to Ozone Trends over China

Chi Li,* Qindan Zhu, Xiaomeng Jin, and Ronald C. Cohen*

ACCESS | Metrics & More | Article Recommendations | Supporting Information

ABSTRACT: In China, emissions of ozone (O_3)-producing pollutants have been targeted for mitigation to reduce O_3 pollution. However, the observed O_3 decrease is slower than/opposite to expectations affecting the health of millions of people. For a better understanding of this failure and its connection with anthropogenic emissions, we quantify the summer O_3 trends that would have occurred had the weather stayed constant by applying a numerical tool that "de-weathers" observations across 31 urban regions (123 cities and 392 sites) over 8 years. O_3 trends are significant ($p < 0.05$) over 234 sites after de-weathering, contrary to the directly observed trends (only 39 significant due to high meteorology-induced variability). The de-weathered data allow categorizing cities in China into four different groups regarding O_3 mitigation, with group 1 exhibiting steady O_3 reductions, while group 4 showing significant ($p < 0.05$) O_3 increases. Analysis of the relationships between de-weathered odd oxygen and nitrogen oxides illustrates how the changes in NO_x, in anthropogenic volatile organic compounds (VOCs), and reductions in fine particulate matter ($PM_{2.5}$) affect the O_3 trends differently in these groups. While this analysis suggests that VOC reductions are the main driver of O_3 decreases in group 1, groups 3 and 4 are primarily affected by decreasing $PM_{2.5}$, which results in enhanced O_3 formation. Our analysis demonstrates both the importance of and possibility for isolating emission-driven changes from climate and weather for interpreting short-term air quality observations.

KEYWORDS: *air quality, ozone pollution, environmental policy, volatile organic compounds, nitrogen oxides, de-weathering of observations*
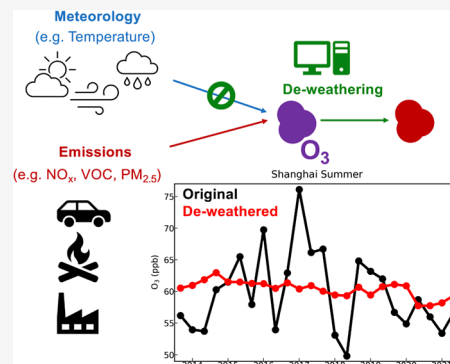
INTRODUCTION

Surface ozone (O_3) pollution is harmful to human health and crop growth.[1−4] In 2019, ambient O_3 was estimated to cause 365,000 premature deaths worldwide, with over a quarter (93,300) in China.[5] From the time of the nationwide deployment of an air quality monitoring network in 2013 through 2019, O_3 across China steadily increased.[6−8] This was especially so during summer when the local production of O_3 is the strongest.[6,9,10] This trend cannot be intuitively understood in light of stringent measures adopted by China beginning 2013 to mitigate O_3, particles, and associated precursor emissions.[11,12] Indeed, policy success is evidenced by reductions in the concentrations of nitrogen dioxide (NO_2)[13,14] and ambient fine particulate matter ($PM_{2.5}$)[11,15] for which emission mitigation policies have been recognized as the dominant driver.[11,12,16,17] In contrast, the lack of success of these policies for reduction of O_3 is disappointing. A variety of causes for failure to reduce O_3 have been reported.[7,18−23] The lack of consensus makes it difficult to assess and predict the most effective policies to reduce O_3 in the future. Recent observations have added to the confusion. In the summer of 2020, there was an unprecedented drop of observed O_3 versus 2019.[8,24] It is unclear whether that signaled a sustainable

transition to a new era of effective O_3 mitigation based on existing policies or it was an anomaly.

This entangled issue arises from the non-linear dependence of O_3 on various anthropogenic and natural factors. O_3 is not directly emitted. It is formed via the photochemical reactions involving atmospheric nitrogen oxides (NO_x), volatile organic compounds (VOCs), and hydrogen oxide radicals (HO_x) (e.g., Figure S1). In particular, O_3 formation exhibits strong non-linear dependence on NO_x and could be promoted or inhibited by NO_x under different chemical regimes[7,25−27] (see also Figure 4). High aerosol loading also affects O_3 by suppressing HO_2.[18,21,28] Meteorological conditions significantly modify O_3 variability by affecting the processes of transport, dilution, and wet and dry deposition.[23,29−32] Meteorology also affects chemistry through altering emissions of NO_x from soils and other sources,[26,33−35] emissions of VOC from the biosphere, evaporative sources and other processes,[26,36] and by affecting
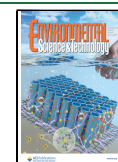
reaction rates that produce and/or consume O_3.[37] Disentangling the meteorological impacts is therefore a pre-requisite for evaluating O_3 responses to emission changes. Apart from model simulations,[29,32,38,39] regression-based weather adjustment/normalization approaches that connect observed O_3 to relevant meteorological parameters have been developed since the 1990s[22,40,41] and provided insightful attributions. These statistical approaches rely strongly on the correctness of the assumed/parameterized relationships and usually cannot accurately represent the pollutant variabilities (especially extreme events).[40,42] Machine learning (ML) instead of traditional statistical regression has received increasing attention due to its inherently non-parametric nature and ability to resemble a complex relationship between a pollutant and its drivers including extremes. Capable of explaining hourly variabilities, ML-based models have been developed to attribute short-term and even episodic changes of air pollutants, including O_3[42−45] and OH.[46,47] Here, we develop an ML-based approach to attribute the recently observed O_3 changes in China and interpret their connections to emissions. This explicit and quantitative connection between emissions and O_3 trends is a unique contribution of this analysis.

Existing methods for separating the contribution of emissions, chemistry, and meteorology to O_3 in Chinese cities include multi-variable regression[6,7,22,48] and chemical transport modeling.[29,32,38] In these studies, the recent increases of summer O_3 pollution were attributed to the combined effects of emissions and meteorology. Different studies reached different conclusions about the attribution. The quantified attribution of effects of meteorology and emission changes varied regionally in these analyses due to the vast land area with various climate zones as well as the rapid but regionally imbalanced economic developments across China. For example, Li et al.[6] attributed about 1/3 of the observed increase (0.7 of the 1.9 ppb/year) of summer O_3 across China to meteorology. In contrast, comparing model simulations with fixed and varying emissions, Liu and Wang[29] found that the rapid increases of O_3 over the urban areas of China were mainly due to emission changes, although variations in meteorology were more determinant over rural areas. However, the specific anthropogenic drivers of these recent O_3 trends remain elusive. Li et al.[18,22] used ground-based data to reveal a strong influence of the $PM_{2.5}$ decrease on the O_3 increase over North China and attributed that response to aqueous uptake of hydroperoxyl radical (HO_2). Their interpretation was supported by model simulations with/without such uptake. In contrast, Tan et al.[19] found that gas-phase chemistry could fully explain HO_x and organic peroxy radical concentrations during a summer campaign near Beijing, questioning the significance of the proposed heterogeneous chemistry on O_3 formation. Other studies[7,21,39] attributed the anthropogenic drivers mainly to gas-phase chemistry affected by NO_x reductions and the non-linear response of O_3 in the VOC-limited regime. Of note, changes in anthropogenic VOC have been relatively less discussed than NO_x or aerosol in these previous studies of Chinese urban O_3. However, VOCs are well known to be important and have been identified as contributors to O_3 trends elsewhere.[26,37,49−51] Although China has initialized regular VOC monitoring plan since 2019, publicly accessible data set is not yet available. Although anthropogenic VOC emissions in China were estimated to change less than NO_x since 2013,[11,52] there is a lack of

observational evidence one way or the other on the role of VOC control in the interpretation of O_3 trends in China.

We examine summer (JJA) and afternoon (13−19 in UTC + 8) O_3 trends during 2014−2021 in 31 Chinese urban regions (123 cities and 392 sites) and develop a ML-based procedure for assessing what would have happened if the weather had stayed constant. Furthermore, we describe changes in the de-weathered response of odd oxygen ($O_x \equiv O_3 + NO_2$) to nitrogen oxides (NO_x) across the 31 regions. These de-weathered changes reveal the effects of changing anthropogenic VOC and decreasing $PM_{2.5}$ on O_x and O_3 trends. The trends and their drivers vary across the cities analyzed. Recognition of these recent emission-driven O_3 trends and their drivers leads to valuable and region-specific insights that should guide future O_3 mitigation policies over urban China.

■ MATERIALS AND METHODS

De-weathering of Observations. We collected 8 years of summer observations of hourly air pollutants (NO_2, O_3, and $PM_{2.5}$) over China along with reanalysis meteorological fields (see details in Section S1). The observations were de-weathered following previous studies.[42−45] Briefly (Figure S2), a ML model (i.e., XGBoost) is built to relate the hourly concentration with time variables (representing emission changes) and meteorological parameters at each site. The time variables include a monotonic time index (time) representing the regular emission trends due to industrialization or environmental regulations, the hour of day representing possible diurnal variabilities in emissions, and the day of week to capture weekly emission cycles. We found that the frequency of employed time index affected the regularity of daily de-weathered NO_2 time series, and allowing too frequent emission variations (e.g., daily frequency) in the XGBoost model brought irregular changes of NO_2 variabilities and weakened the weekly cycles (Figure S3). We adopted 1/2 month (i.e., 48 time indices over the 8 years) in the final XGBoost model to avoid potential overfitting, while maintaining the expected variation driven by emission trends. The nine meteorological fields (Section S1) are consistent with those used by Shi et al.[43] and are the most relevant for variation of surface air pollutant concentrations.

A five-fold cross-validation[53] (Section S4) is employed to evaluate the XGBoost models for 828 sites that have long-term observations (Section S1). We eliminated sites with the coefficient of determination (R^2) <0.45 for hourly NO_2 or <0.65 for hourly O_3 to ensure model accuracy and to support reliable de-weathering (690 sites remain after this strict filter). We further screened sites with strong inter-annual variability of background O_3 (see Section S2, 525 sites remaining). Finally, we identified 31 conventional city clusters that comprise 75% (392) of these qualified sites (Figure S4 and Table S1) for trend analysis. Their definitions were primarily from authorized development planning documents such as the NDRC.[54] The distribution of qualified sites (i.e., including a larger domain where sites are sparse) was also considered. City-level time series were also used to slightly adjust the lists of included cities, so that NO_2 and O_3 trends within each region are similar (e.g., Figure S4). For each region, years that contain <2/3 of the total qualified sites are eliminated from the analysis to guarantee the representativeness of the calculated time series and trends of regional mean air quality.

Figure S5 shows the distribution of R^2 metrics of comparison pairs during cross-validation, between the observed and

predicted hourly concentrations across the 392 sites with data sets that are adequate for this analysis. The overlapping R^2 distributions found when employing varying time index frequencies (1/2 and 1/4 months) further confirm the validity of the employed time indices (i.e., model performance stops improving after 1/2 month). Overall, site-specific cross-validation R^2 (5−95th percentiles) of 0.47−0.70 for NO_2, 0.69−0.81 for O_3, and 0.57−0.77 for $PM_{2.5}$ are achieved. These values are smaller by 0.1−0.2 than in Vu et al.,[44] in part due to the inclusion of only summer and afternoon data in this study. The meteorological variability as well as effects on concentration variability are thereby reduced relative to Vu et al.[44] who investigated data at all hours and seasons. Figure S6 shows the feature importance of each predictor in the XGBoost models for each pollutant, summarized from all the investigated sites. The time index (i.e., emission regulations) is the largest contributor to the prediction of NO_2 and $PM_{2.5}$, while meteorological factors affect the prediction less. Surface temperature is the most important for O_3, as it significantly affects biogenic/soil emissions and chemical reaction rates. These rankings of predictor importance are consistent with expectations, as well as with the findings of previous de-weathering studies.[43,44] In summary, the derived XGBoost models successfully captured the summer and afternoon O_3 variabilities and their connections to specific drivers. The models' predictive power (i.e., $R^2 > 0.7$) and representativeness of O_3 variability at hourly frequency are substantially stronger than prior model simulations (e.g., Table 2 of Liu and Wang[29]) and multi-linear regressions (e.g., Figure S4 of Li et al.[6]) at daily/monthly scales, supporting the further application of the model results to attribution of O_3 trends to emission and meteorological effects. Similarly, the robust predictability of NO_2 and $PM_{2.5}$ variabilities by the XGBoost models supports the further connection of de-weathered O_3 changes to relevant emissions.

We then used the trained XGBoost models (f) to predict the de-weathered concentrations (C^d) of NO_2, O_3, and $PM_{2.5}$ for each hour (i), as averaged from the ensemble predictions using the corresponding time variables (T_i) and all possible weather conditions [W_k, k varies over n (at most 736) days in the 8 summers] at the same hour of the day (Figure S2).

$$C_i^d = \frac{\sum_{k=1}^n f(T_i, W_k)}{n} \tag{1}$$

Similarly, the de-weathered NO is estimated as the ensemble means of steady-state calculated NO[55] using the corresponding de-weathered NO_2 and O_3, and all possible temperatures at the same hour of the day. In this manner, we predict the concentration as if the weather were repeated every day during all the eight summers, while the emissions varied realistically. The ML de-weathering technique has been successfully adopted to investigate both multi-year[42,44] and episodic[43,45] air quality changes and is especially a powerful tool to isolate changes due to emissions alone. Figure S7 shows that the strong temperature dependence of O_3 has been massively reduced over Shanghai in the de-weathered data. The reduced sensitivity to temperature is uniformly observed in the de-weathered O_3 over all the other regions (not shown).

Chemical Mechanism Calculation. We employed a single-box model calculation, including emissions of NO_x and key photochemical reactions (Figure S1), to investigate the theoretical responses of O_x to NO_x and its changes in

response to variations of VOC and $PM_{2.5}$. The model configuration can be found in previous studies,[56,57] from which we further added Reactions R11 and R12 (Figure S1) to facilitate quantifying the effects on O_3 formation from $PM_{2.5}$ and existing background O_3.

$$PM_{2.5} + HO_2 \rightarrow H_2O_2 \tag{R11}$$

$$O_3 + H_2O \xrightarrow{h\nu} 2OH \tag{R12}$$

Reaction R12 is a combination of O_3 photolysis to O^1D and sequential OH formation from O^1D and water vapor. For Reaction R11, the reactive uptake coefficient (γ) of HO_2 by $PM_{2.5}$ is set to 0.2 following Li et al.[18] The $PM_{2.5}$ mass concentration is converted to the surface area concentration assuming a monodispersed size of 0.8 μm and a density of 1 g/cm^3. For Reaction R12, the OH yield is estimated assuming $J(O^1D)$ of 2×10^{-5} s^{-1}, 3% of O^1D to form OH, and furthered scaled by 1.25 to account for other sources of OH production.

The temperature was set as 298 K, and wind was not included while we added depositional sinks for NO_x and O_3 (first order loss rate of 10^{-5} s^{-1}) to facilitate steady-state in the single box. Each simulation comprises 25 distinct values for NO_x emissions to derive a series of steady-state O_x and NO_x concentrations (e.g., gray circles in Figure 4). Initial O_3 (25 ppb), VOC (25 ppb, equivalent to VOC reactivity of 15 s^{-1}), and $PM_{2.5}$ (50 μg/m^3) were set for the base simulation and varied in each sensitivity simulation (e.g., colored lines in Figures 4 and S13) to illustrate their effects on the O_x−NO_x relationship. All these settings represent typical pollution scenarios in summer over China and other urban regions.[18,25,58,59]

■ RESULTS

Summer Trends in O_3, NO_2, and O_x across China. Surface observations of afternoon (13−19 in UTC + 8) NO_2 and O_3 in 31 Chinese urban regions (Table S1 and Figure S4) show distinctive changes during the summers (June, July, and August) of 2014−2021 (e.g., Figures 3 and S8). However, the trends are masked by variability of the weather. Figure 1 (open circles) shows the 8 year evolution of monthly mean NO_2 and O_3 over Shanghai. NO_2 exhibits decreases averaging −0.4 ± 0.3 ppb/year through the entire period. In contrast, O_3 shows fluctuating increases by about 0.9 ± 2.4 ppb/year in the early part of the record (2014−2018) and decreases afterward (−1.1 ± 2.4 ppb/year during 2018−2021). All these trends and the O_3 trend over 2014−2021 (−0.3 ± 1.0 ppb/year) are insignificant ($p \geq 0.05$, see also Figure S8). O_3 trends over such short periods are subject to the strong monthly and inter-annual variabilities determined by the combined changes in precursors and meteorology. For example, from 2014 to 2018, there was a trend of surface temperature of 1.0 ± 0.8 K/year ($p < 0.05$) (Figure 1, red).

The significant modulations of O_3 inter-annual variability by temperature are widespread across China, as indicated by Figure 2, showing coincident yearly difference maps of surface temperature (background, from the ERA5 reanalysis) and O_3 (circles). The inter-annual temperature changes and the concurrent changes of O_3 show similar spatial patterns, with positive spatial correlations (0.2−0.6). The abnormally high temperatures during two consecutive years (2017 and 2018) over North China have been identified as a significant driver of O_3 increases.[6,29,38] The temperature decreased in 2020 and
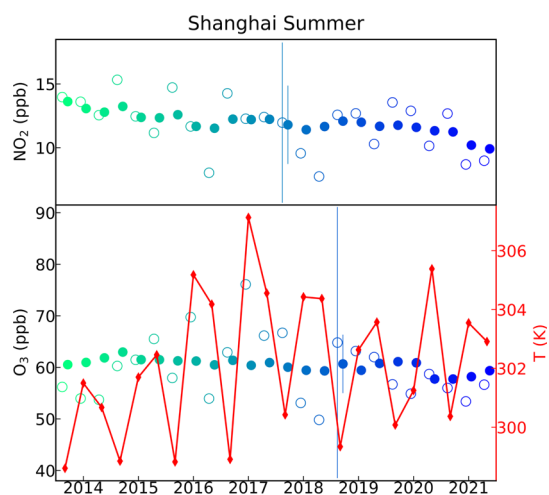
Figure 1. Evolution of summer NO_2 and O_3 over Shanghai, China. Circles represent the monthly means of the original (empty) and de-weathered (filled) observations during the afternoons (13−19 in UTC + 8) of June−August, 2014−2021 (x-ticks at each July). The error bars represent typical standard deviation of hourly observations in each month. Collocated monthly mean 2 m temperature (red) from the ERA5 reanalysis is superimposed in the O_3 panel.

then increased in 2021, making it challenging to interpret recent O_3 changes.

The ML-based de-weathering approach[42−45] isolates trends (filled circles in Figure 1) that are solely due to changing emissions. The de-weathering reasonably reduces the monthly variability of the observed mixing ratios especially for O_3. For example, the abnormally high O_3 in the July of 2016 and 2017, which were associated with high temperatures (Figure 1, red), does not appear as an anomaly in the de-weathered data

(Figure 1, filled circles). Furthermore, the standard deviations of hourly O_3 within each month are reduced from >20 to <8 ppb. This is consistent with the significantly reduced dependence of the hourly O_3 concentration on ambient temperature after de-weathering (Figure S7). Both the NO_2 (-0.3 ± 0.1 ppb/year) and O_3 (-0.4 ± 0.1 ppb/year) trends after the de-weathering are significant ($p < 0.05$) and negative. Such strikingly different interpretations of O_3 trends highlight the strong modulation of the emission-driven trends by meteorology.

Figure 3 shows the de-weathered summer trends in O_3, NO_2, and odd oxygen ($O_x \equiv O_3 + NO_2$) over all the 31 urban regions (392 sites). Compared with the raw observational trends (Figure 3 vs S8 and S4 vs S9), one notable difference of the de-weathered analysis is that many more sites and cities have trends that are statistically significant (i.e., filled vs empty for bars and circles). This observation is more pronounced for O_3 than for NO_2, as meteorological effects on NO_2 are relatively weaker (e.g., Figure S6). Particularly, the number of sites with significant ($p < 0.05$) O_3 trends increases from 39 (Figure S9) to 234 (Figure S4, 51 decreases and 183 increases). The de-weathered regional and monthly NO_2 and O_3 time series appear to exhibit more steady and less fluctuating changes, in contrast to the stronger variabilities in the original data (Figure S10).

Based on the de-weathered O_x trends and significance, we categorize the 31 regions (123 cities) into four characteristic groups (Figures 3 and S4):

Group 1: 5 regions (10 cities) from Changchun (CC) to Beijing (BJ), where the de-weathered O_x exhibits significant ($p < 0.05$) decreases [from -0.8 ± 0.4%/year in Ningbo (NB) to -2.1 ± 0.7%/year in CC] across 2014−2021 (i.e., the filled green bars in Figure 3). The concurrent O_3 trends (i.e., purple
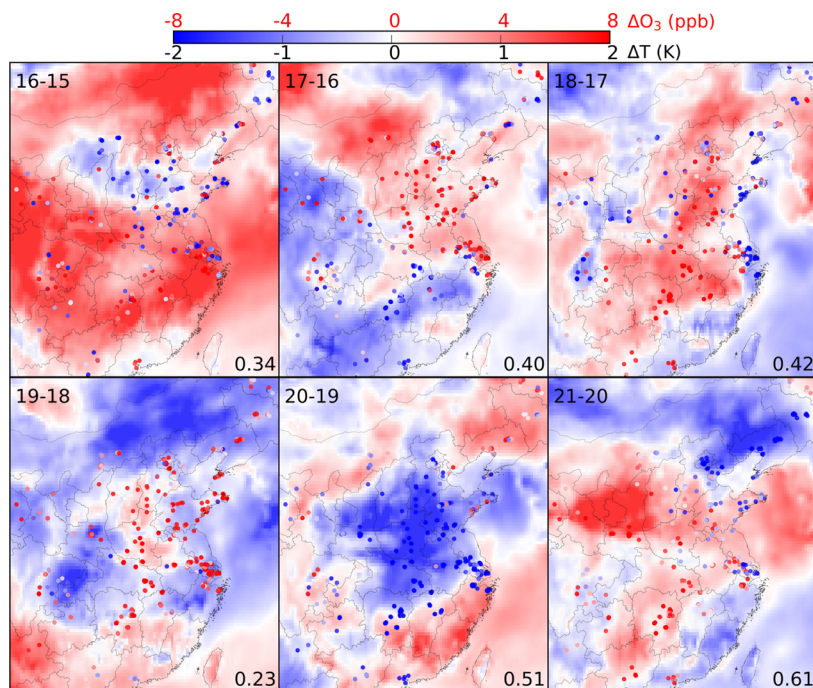
Figure 2. Strong effects of surface temperature on O_3 inter-annual variation across China. Circles represent the difference in the summer afternoon mean O_3 concentration for each year vs the previous year, plotted on the corresponding differences in surface (2 m) temperature from ERA5 reanalysis (background). Spatial correlations between them are inserted on the bottom-right of each panel. Differences prior to 2015 are not shown due to significantly reduced site density.
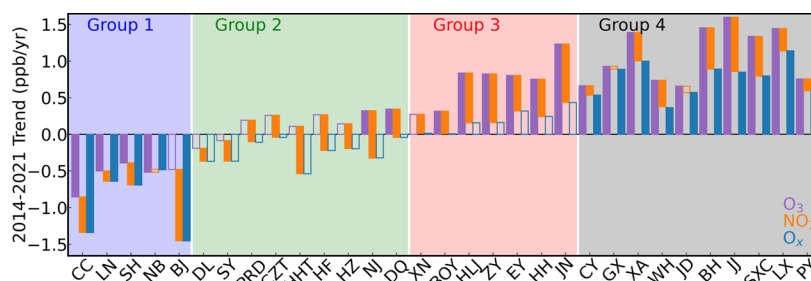
Figure 3. Trends of de-weathered summer O_3, NO_2, and O_x over China. Bars (filled: $p < 0.05$; empty: $p \geq 0.05$, color-coded for different species) represent fitted linear trends over 2014−2018, based on monthly mean mixing ratios for each urban region. The four groups of regions (group 1: significant O_x reductions; group 2: insignificant O_x reductions; group 3: insignificant O_x increases; and group 4: significant O_x increases) are indicated by the shaded background colors.

bars in Figure 3) are all negative (from $-0.6 \pm 0.5\%$/year in BJ to $-1.6 \pm 0.7\%$/year in CC) and mostly significant ($p < 0.05$), except for BJ ($p = 0.054$). De-weathered NO_2 trends in group 1 (i.e., red bars in Figure 3) are also negative and significant ($p < 0.05$), except for NB ($0.4 \pm 1.0\%$/year, $p = 0.5$). Median decreases in NO_2 were $-2.5 \pm 0.6\%$/year over these 8 years.

Group 2: 9 regions (27 cities) from Dalian (DL) to DianQian (DQ), where the de-weathered O_x shows insignificant ($p \geq 0.05$) decreases. The NO_2 trends are all significant ($p < 0.05$) and negative [from $-2.1 \pm 1.4\%$/year in DL to $-8.3 \pm 1.7\%$/year in Hohhot (HHT)], while O_3 trends start to reverse from negative to positive in group 2 and finally become significant ($p < 0.05$) for Nanjing (NJ, $0.5 \pm 0.3\%$/year) and DQ ($0.8 \pm 0.4\%$/year).

Group 3: 7 regions (32 cities) from Xiangnan (XN) to Jinan (JN), where the de-weathered O_x reveals insignificant ($p \geq 0.05$) increases. Both the increasing O_3 [from $0.5 \pm 0.3\%$/year in BaoOrYu (BOY) to $1.7 \pm 0.6\%$/year in Heilongjiang (HLJ)] and decreasing NO_2 [from $-4.1 \pm 1.3\%$/year in BOY to $-9.1 \pm 1.1\%$/year in Zhongyuan (ZY)] are significant ($p < 0.05$), with the sole exception of O_3 in XN ($0.6 \pm 0.5\%$/year, $p = 0.053$).

Group 4: 10 regions (54 cities) from ChuanYu (CY) to Poyang (PY), where the de-weathered O_x increases [from $0.5 \pm 0.4\%$/year in Wuhan (WH) to $1.8 \pm 0.5\%$/year in Guangxi (GX)] and the trends are significant ($p < 0.05$). O_3 increases [from $1.1 \pm 0.4\%$/year in Jiaodong (JD) to $2.4 \pm 0.4\%$/year in Longxi (LX)] and NO_2 decreases [from $-0.7 \pm 2.7\%$/year in GX to $9.0 \pm 1.2\%$/year in JinJi (JJ)] are also significant, with two exceptions for NO_2 (GX and JD).

Figure S4 (bottom) shows the locations of the four groups of regions and the included sites. Under normalized weather during 2014−2021, group 1 sites exhibit reductions of summer O_3 and are mainly located over the Northeast (CC and LN) and eastern China (SH and NB) as well as the Capital Beijing. Groups 3 and 4 are regions with steadily increasing O_3 pollution and are located across inland China, especially the most polluted North China Plain (i.e., BH, JJ, JN, JD, XA, ZY, EY, and HH). O_3 increases in these regions were consistently reported in previous studies.[6,18,22] The positive O_3 trends after de-weathering are also consistent with Li et al.[6] who showed that emission changes are the dominant driver of these O_3 increases over the North China Plain. Group 2 roughly characterizes the intermediate regions, usually bordering group 1 and group 3 regions.

The regional and monthly mean NO_2 and O_3 after de-weathering have various correlations (Figure S10), which evolves from positive in group 1 ($0.20-0.72$, median: 0.47) to

negative in groups 3 and 4 (-0.05 to -0.79, median: -0.55). These variable correlations suggest different responses of O_3 to emission controls in different region groups, which will be further elaborated using the de-weathered $O_x - NO_x$ relationship (next section).

Figure S11 indicates that the magnitudes of temporal trends for all the regions are tightly correlated with those arrived without de-weathering ($R^2 > 0.8$), implying that emission changes explain most of the 8 year trends. The small number of significant trends in the O_3 data without de-weathering indicates the meteorological modulations add substantial noise and intervene in the clear interpretation of O_3 trends due to emission policies.

Figure S12 shows that since 2019, negative trends in O_3 (264 sites, 106 significant) occur widely across China in the de-weathered observations. The original data (327 negative trends, 20 significant) again contain O_3 trends which are mostly not significant, partially driven by the strong temperature anomalies (Figure 2). These trends suggest a reversal tendency of dominant O_3 changes in China, which could be related to the second-phase of the "Blue-Sky-War" action that extended and strengthened the clean-air actions during 2013−2017.[13,60,61] The potentially reduced industrial production in China during the global COVID pandemic (2020−2021) might further reduce relevant activities that release O_3 precursors to the atmosphere.[62] Continuous surveillance and de-weathering of air quality observations across China will be required to further confirm and evaluate if this trend reversal will be sustained.

In summary, the de-weathered O_3 and NO_2 show robustness against meteorological variability, with clearly recognizable and more statistically significant trends than the data without de-weathering. Over 2014−2021, the number of sites with significant ($p < 0.05$) O_3 trends increases six-fold, while only three regional O_3 trends are significant before de-weathering (Figure S8). Such sharp differences highlight the effectiveness of de-weathering at isolating the short-term response of O_3 to emission changes.

$O_x - NO_x$ Relationship and Implications for Future O_3 Trends. The derived emission-driven O_3 changes can be interpreted using the changes in the de-weathered responses of odd oxygen (O_x) to nitrogen oxides (NO_x). As O_3 and NO_2 inter-convert rapidly (~100 s) during the daytime, we define the sum of O_3 and NO_2 as O_x, a quantity that is conserved on longer time scales. The O_x variation in response to NO_x and VOC has been studied extensively.[25,26,35,37] Long-term changes in O_x are a robust indicator of changes in O_3 production, but we also note that decreasing O_x can be associated with variable

changes in O_3 if driven by NO_x reductions.[26] Figure 4 is a summary of expectations from evaluation of the chemical
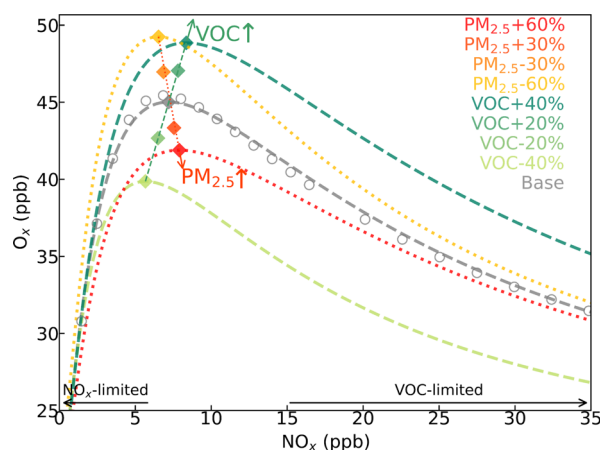
Figure 4. Changes in O_x–NO_x relationship in response to changing VOC and $PM_{2.5}$. Gray circles represent O_x and NO_x concentrations from the base scenario calculation, which has a $PM_{2.5}$ concentration of 50 $\mu g/m^3$ and a VOC reactivity of 15 s^{-1}, and the gray curve shows the associated log−normal fit ($R^2 = 0.997$). The diamond point is the peak (mod) of the log−normal curve, representing the separation of the NO_x-limited (left) and VOC-limited (right) regimes. For other scenarios (color-coded), either $PM_{2.5}$ (yellow to red, dotted) or VOC (light to dark green, dashed) is varied, and only the log−normal fits ($R^2 > 0.996$) and/or their peaks (diamonds) are shown for brevity.

mechanism (Materials and Methods and Figure S1). Since O_3 over China has been identified to respond sensitively to changes in $PM_{2.5}$,[18,22] we also included the process of aqueous HO_2 uptake by $PM_{2.5}$ in the calculation (i.e., Reaction 11 in Figure S1. See the Materials and Methods section for more details).

There are four factors that must be disentangled to understand the de-weathered O_3 trends. These are the background O_3, the NO_x, the VOC, and the $PM_{2.5}$. Figure 4 shows the effects of the three emission-relevant factors, NO_x, VOC, and $PM_{2.5}$. At fixed values of VOC, $PM_{2.5}$, and background O_3 (e.g., the base case in gray), O_x increases with NO_x within the NO_x-limited regime (left), where the abundance of organic peroxy radicals (RO_2) is sufficient that the production rate of O_x (i.e., Reactions 5 and 9 in Figure S1) is nearly linear with NO_x and insensitive to VOC. At the VOC-limited regime (right), increasing NO_x consumes HO_x through the $OH + NO_2$ termination reaction (i.e., Reaction 3 in Figure S1) and therefore reduces O_x production, resulting in an anti-correlation between O_x and NO_x. Following previous studies,[7,63] we find that a log−normal function (e.g., the gray curve) could almost perfectly ($R^2 > 0.995$) describe this O_x–NO_x behavior across both regimes, and the peak (i.e., the diamond points in Figure 4) of the log−normal fits could be the benchmark to separate the two regimes.

In this model, increasing VOC (i.e., from light to dark green curves in Figure 4) increases the O_x yields in the VOC-limited regime, as well as extends rightward the NO_x concentration range of the NO_x-limited regime. These effects together shift the O_x–NO_x curve toward the upper right (i.e., the direction of the green arrow in Figure 4), as represented by the shifts of the transition points (diamonds). Increasing $PM_{2.5}$ (i.e., yellow to red curves in Figure 4) enhances the HO_x sink and decreases the O_x production without consuming NO_x. The

effect is weaker at higher NO_x concentrations in the VOC-limited regime (i.e., converges at the right). As a result, the O_x–NO_x curves as well as the transition points shift lower-rightward with increasing aerosol (i.e., the red arrow in Figure 4).

Changes to the background O_3 add an additional non-local contribution to O_3 trends. Figure S13 further shows how changing the background O_3 will also reshape the O_x–NO_x relationship even without changes in VOC or $PM_{2.5}$. This is due to the positive feedback of enhanced HO_x production (i.e., Reaction 12 in Figure S1) at higher O_3. To focus on the discussion of potential changes in O_x–NO_x due to emissions, we estimated the background O_3 for each year (Figure S14) and filtered sites with yearly background O_3 varying by over 20% (e.g., Figure S15, left).

This conceptual model is applied to interpretation of the de-weathered observations (see details in Section S2). Figure 5
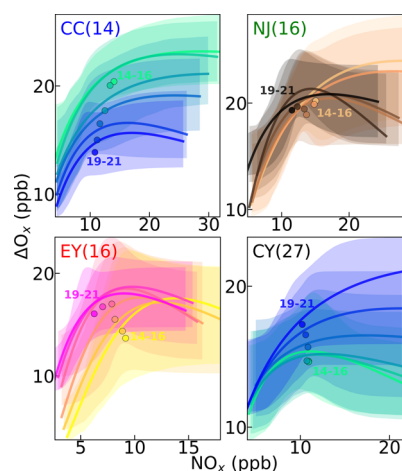
Figure 5. Changes of de-weathered O_x–NO_x relationship over four regions. Over CC, NJ, EYu (EY), and CY, lines represent the log−normal fits of 3 year (colored from light to dark) hourly O_x and NO_x concentrations after de-weathering, and shadings are their 25−75% confidence intervals. The number of included sites is displayed in the bracket following the region name. The O_3 background concentrations for each region were subtracted from total O_x on the y-axis to represent changes in the net O_x production (ΔO_x). Points placed the 3 year mean O_x and NO_x for each period.

shows the distributions of 3 year moving summer O_x–NO_x relationships, as derived from the de-weathered observations over four regions that are representative of the four city groups (Figure S16 shows the results over all the 31 regions), each belonging to one region group categorized in the previous section.

Over CC (upper-left), the O_x–NO_x curves as well as the 25−75% ranges exhibit a continuous decrease and a lower-leftward shift of the fitted log−normal lines. As $PM_{2.5}$ also decreased continuously (Figure S4), this downward shift of de-weathered O_x–NO_x should be a result of decreasing VOC. Similarly steady downward shifts of the O_x–NO_x curves are observed in the other group 1 regions (Figure S16). This shows that VOC emission reductions were important to the long-term O_3 reductions in the group 1 (de-weathered) O_x and O_3. These effective O_3 reductions following VOC emission controls also explain the positive correlations of the O_3 and NO_2 time series (Figure S10) in group 1 since NO_2 has been simultaneously reduced during the emission regulation

activities. Future VOC regulations will remain a central component for O_3 mitigation over these regions according to this analysis, especially over the two southern cities (SH and NB) where the mean NO_x (i.e., circles in each panel of Figure S16) concentration is in the VOC-limited regime, and reducing NO_x alone (i.e. leftward shifts following the same curve) will not lead to decreases in O_x or O_3. Over the other three northern regions (CC, LN, and BJ), however, the mean NO_x locates between the transition and NO_x-limited regime in the historical de-weathered data records, and so, future NO_x reductions will also further contribute to O_3 improvements in these cities.

Over NJ (upper-right of Figure 5), the de-weathered O_x- NO_x relationship exhibits reductions of O_x that we identify as occurring in the VOC-limited (right) regime. At the same time, we also identify increases of O_x in the NO_x-limited regime (left). The 25−75% ranges of the curves are largely invariant over time even though the de-weathered NO_x decreases. We interpret these observations to indicate that VOC reductions (causing the O_x reductions on the right) were counteracted by the concurrent decreases in $PM_{2.5}$ (leading to the O_x increases on the left, Figure S4), in the net, yielding small changes in the mean O_x. Many other group 2 regions (SY, HHT, HF, HZ, and DQ) do not exhibit significant changes in their O_x despite the large changes in NO_x (Figure S16). We interpret this result as due to similar counteracting effects of VOC and $PM_{2.5}$. For these regions, more stringent regulations on VOC (to reduce O_x production rates and overcome the increased O_3 production occurring due to $PM_{2.5}$ decreases) are required to achieve future O_3 reduction. Exceptions are found over DL, PRD, and CZT (also in group 2), where stronger changes of O_x are observed in the VOC-limited regime relative to the NO_x-limited regime, namely, VOC changes are already driving these changes in the de-weathered O_x-NO_x relationship. Over DL and CZT, the insignificant trends in O_x and O_3 (Figure 3) are consistent with the non-monotonic changes of the O_x production in the VOC-limited regime (i.e., decrease first and increase later after 2018−2019), indirectly implying variation in emissions of VOC. Reinforcing VOC controls will likely migrate these two regions into group 1 in the future. Over PRD, steady VOC reductions can be inferred from the O_x-NO_x curve, while most de-weathered observations are distributed toward the NO_x-limited regime (reflected by the location of mean O_x and NO_x), and responses of O_3 and O_x changes to these VOC regulations were relatively weaker. Controlling NO_x emissions thus will be more important for future O_3 regulations in PRD.

The main feature of such joint/counteracting VOC and $PM_{2.5}$ control of the O_x-NO_x curves over most group 2 regions also extends to three regions (XN, BOY, and HLJ, Figure S16) of group 3, except that now the $PM_{2.5}$ effects are seen to be strong enough to surpass the VOC effects, resulting in overall O_x increases (see also Figure 3). As this trend continues, for EYu (EY, lower-left of Figure 5) and most of the other regions in groups 3 and 4 (i.e., from ZY to PY in Figure S16, except for CY), the O_x-NO_x curves as well as the 25− 75% ranges finally become controlled by $PM_{2.5}$ reductions (Figure S4). This is consistent with the continuous O_x increases and upper-leftward shifts of the fitted log−normal lines. The VOC effects, on the other hand, are less notable in the de-weathered data across the investigated years. These regions are mainly located in the eight city clusters across the North China Plain, where O_3 and $PM_{2.5}$ pollution are both the

most severe in China (e.g., Figure S4), as well several regions near this plain (Figure S4) at the northwest (LX), south (WH and PY), and southeast (SXC). The significant O_3 increases (Figure 3) driven by $PM_{2.5}$ reductions following emission regulations lead to the negative correlations of O_3 and NO_2 time series (Figure S10) over these regions. In recent years (i.e., comparing the 2018−2020 with the 2019−2021 O_x-NO_x curves in Figure S16), such $PM_{2.5}$-driven O_x-NO_x shifts within the NO_x-limited regime were reduced (except GX), relative to the more notable O_x increases in earlier years. This suggests that the $PM_{2.5}$ effects on O_x-NO_x are less important in recent years as $PM_{2.5}$ dropped significantly (Figure S4). Synthesized from these observations, we conclude that in the future, particulate pollution will be less critical for O_3 production, and the effectiveness of VOC and NO_x regulations to reduce O_3 will instead emerge and increase, similar to the cities in groups 1 and 2.

Over CY (lower-right of Figure 5), the O_x-NO_x relationship is dominantly characterized by continuous increases of O_x production as well as an upper-rightward shift, indicative of steady VOC emission growth. This is the only region among the 31 investigated (Figure S16) that reveals such VOC-driven O_3 increases. Overturning this inferred increase of anthropogenic VOC is thus the prerequisite for O_3 mitigation in this area.

■ DISCUSSION

The complex dependence of O_3 on emissions and meteorology could blur and confuse the interpretation of O_3 trends, especially for the short period that O_3 has been monitored over China. We show that applying numerical de-weathering to the air quality data is a powerful step to simplify describing and understanding the O_3 time series. After the de-weathering, cities in China are more clearly positioned in different phases (as characterized mainly by the groups in Figure 3) regarding O_3 mitigation. While O_3 control policies that are aiming to produce cleaner air have been effective across group 1 regions, the roles of VOC and $PM_{2.5}$ induced a variety of trends in O_x and O_3 in the other regions.

These insights are derived from our unique analysis of O_x- NO_x relationships in response to emission regulations using the de-weathered observations. We show that there was a major role for VOC and aerosol changes in regulating O_3 over China. We inferred that VOC reductions contributed to both the O_3 reductions in group 1 regions, as well as competed with the $PM_{2.5}$ effects over the group 2 regions. These regions in groups 1 and 2 comprise the traditionally recognized nation-level economic centers of Beijing (BJ), Yangtze River Delta (SH, NB, HZ, and NJ), and Guangdong Province (PRD), where vehicle emission standards (e.g., "China 5" and "China 6") were enforced several years before the rest of China.[64] Ambient VOC measurements have also revealed long-term reductions due to emission controls over Beijing (2005− 2011), Shanghai (2006−2016), and Shenzhen (close to the PRD region, 2014−2019),[65−67] consistent with the inferred reductions of anthropogenic VOC (Figure S16). The other regions of groups 1 and 2 include the northeastern China (CC, LN, SY, and DL). As the historical "rust belt" before 1980s, these cities somehow had maintained the slowest GDP growths across China[68] and witnessed millions of population loss in the last decade.[69] A recent emission inventory also suggests that the Northeast China dominantly had decreasing industrial VOC emissions during 2013−2019,[70] consistent

with the relatively stalled economy and the inferred VOC reductions. The rest of group 2 regions (CZT, HHT, HF, and DQ) exhibit unsteady or unclear VOC changes from the O_x–NO_x graphs (Figure S16), likely driven by counteraction between cleaner vehicles and rapid growing emissions from industry and solvent use[52] that differs year-by-year. Finally, the analysis over CY uniquely indicates steady increase of VOC, consistent with Simayi et al.[70] that implies recent increases of industrial VOC emissions over this region (as a new nation-level economic center since 2010s) were among the strongest across China. Notably, these unprecedentedly detailed insights build a broad connection of current O_3 mitigation over China to historical success experienced over the United States during the last three decades,[26,49,51] both indicating strong dependence on effective VOC controls.

Our analysis of de-weathered observations also clarifies the effects of $PM_{2.5}$. $PM_{2.5}$ reductions reducing the uptake of HO_x have been proposed as a trigger for the recent O_3 increases over the North China Plain.[18,22] Our analysis confirms this effect (i.e., the upper-leftward shifts of the O_x–NO_x curves) from an independent perspective, especially for cities in groups 3 and 4. We also further identified that such $PM_{2.5}$ effects were reduced to be less discernible in recent years (e.g., since 2019), consistent with model simulations and observed O_3–$PM_{2.5}$ relationships,[7,18,21] which suggested that this $PM_{2.5}$ effect on O_3 was only significant over strongly polluted (i.e., $PM_{2.5} > 40$ $\mu g/m^3$) scenarios. Future O_3 mitigations over China will be less affected by $PM_{2.5}$. Conversely, future reductions of VOCs will become increasingly important for these cities, once $PM_{2.5}$ is low enough to become unimportant to O_3.

It is unclear if the investigated 8-year weather would be representative of the future climate, although the projected more frequent summer temperature extremes[71,72] should further interfere with the effectiveness of O_3 mitigation policy. With the emergence of high-resolution and realistic emission inventories, comparing these observational-based emission driven trends with simulations should reconcile observations and models and provide additional quantitative insights and guidance for regulatory policy, no matter what changes occur in future weather or climate.

■ ASSOCIATED CONTENT

ⓢ Supporting Information

The Supporting Information is available free of charge at https://pubs.acs.org/doi/10.1021/acs.est.2c03315.

> Complementary introduction of materials and methods, species and chemical reactions in the chemical mechanism calculation, illustration of the de-weathering approach, de-weathered and original NO_2 over one site in Shanghai, 2014-2021 trends of three pollutants, distribution of cross-validation R^2, importance of predictor features in XGBoost models, dependence of O_3 concentration on the surface temperature, 8 year changes of de-weathered and original NO_2 and O_3, comparison of original and de-weathered trends, 2019−2021 trends of three pollutants, illustration of O_3 background determination, and details about the urban regions (PDF)

■ AUTHOR INFORMATION

Corresponding Authors

Chi Li − *Department of Chemistry, University of California, Berkeley, Berkeley, California 94720, United States;* Present Address: Department of Energy, Environmental and Chemical Engineering, Washington University in St. Louis, St. Louis, MO 63130, USA; ⓞ orcid.org/0000-0002-8992-7026; Email: lynchlee90@gmail.com

Ronald C. Cohen − *Department of Chemistry, University of California, Berkeley, Berkeley, California 94720, United States; Department of Earth and Planetary Science, University of California, Berkeley, Berkeley, California 94720, United States;* ⓞ orcid.org/0000-0001-6617-7691; Email: rccohen@berkeley.edu

Authors

Qindan Zhu − *Department of Earth and Planetary Science, University of California, Berkeley, Berkeley, California 94720, United States;* ⓞ orcid.org/0000-0003-2173-4014

Xiaomeng Jin − *Department of Chemistry, University of California, Berkeley, Berkeley, California 94720, United States;* ⓞ orcid.org/0000-0002-6895-8464

Complete contact information is available at:
https://pubs.acs.org/10.1021/acs.est.2c03315

Author Contributions

The manuscript was written through contributions of all authors. The conceptualization was initialized by C.L. and R.C.C. The methodology was developed by C.L. and Q.Z. C.L. performed the visualization of the results, which were analyzed by all the authors. C.L. wrote the original draft. All authors have reviewed, edited, and given approval to the final version of the manuscript.

Notes

The authors declare no competing financial interest.

■ ACKNOWLEDGMENTS

■ REFERENCES

(1) Lefohn, A. S.; Malley, C. S.; Smith, L.; Wells, B.; Hazucha, M.; Simon, H.; Naik, V.; Mills, G.; Schultz, M. G.; Paoletti, E.; De Marco, A.; Xu, X.; Zhang, L.; Wang, T.; Neufeld, H. S.; Musselman, R. C.; Tarasick, D.; Brauer, M.; Feng, Z.; Tang, H.; Kobayashi, K.; Sicard, P.; Solberg, S.; Gerosa, G. Tropospheric Ozone Assessment Report: Global Ozone Metrics for Climate Change, Human Health, and Crop/Ecosystem Research. *Elementa* **2018**, *6*, 27.

(2) Cohen, A. J.; Brauer, M.; Burnett, R.; Anderson, H. R.; Frostad, J.; Estep, K.; Balakrishnan, K.; Brunekreef, B.; Dandona, L.; Dandona,

R.; Feigin, V.; Freedman, G.; Hubbell, B.; Jobling, A.; Kan, H.; Knibbs, L.; Liu, Y.; Martin, R.; Morawska, L.; Pope, C. A.; Shin, H.; Straif, K.; Shaddick, G.; Thomas, M.; van Dingenen, R.; van Donkelaar, A.; Vos, T.; Murray, C. J. L.; Forouzanfar, M. H. Estimates and 25-Year Trends of the Global Burden of Disease Attributable to Ambient Air Pollution: An Analysis of Data from the Global Burden of Diseases Study 2015. *Lancet* **2017**, *389*, 1907−1918.

(3) Shindell, D.; Kuylenstierna, J. C. I.; Vignati, E.; van Dingenen, R.; Amann, M.; Klimont, Z.; Anenberg, S. C.; Muller, N.; Janssens-Maenhout, G.; Raes, F.; Schwartz, J.; Faluvegi, G.; Pozzoli, L.; Kupiainen, K.; Höglund-Isaksson, L.; Emberson, L.; Streets, D.; Ramanathan, V.; Hicks, K.; Oanh, N. T. K.; Milly, G.; Williams, M.; Demkine, V.; Fowler, D. Simultaneously Mitigating Near-Term Climate Change and Improving Human Health and Food Security. *Science* **2012**, *335*, 183−189.

(4) Turner, M. C.; Jerrett, M.; Pope, C. A., 3rd; Krewski, D.; Gapstur, S. M.; Diver, W. R.; Beckerman, B. S.; Marshall, J. D.; Su, J.; Crouse, D. L.; Burnett, R. T. Long-Term Ozone Exposure and Mortality in a Large Prospective Study. *Am. J. Respir. Crit. Care Med.* **2016**, *193*, 1134−1142.

(5) Health Effects Institute, Institute for Health Metrics and Evaluation. State of Global Air 2020. 2020, https://www.stateofglobalair.org/sites/default/files/documents/2020-10/soga-2020-report-10-26_0.pdf (accessed Nov 2, 2021).

(6) Li, K.; Jacob, D. J.; Shen, L.; Lu, X.; De Smedt, I.; Liao, H. Increases in Surface Ozone Pollution in China from 2013 to 2019: Anthropogenic and Meteorological Influences. *Atmos. Chem. Phys.* **2020**, *20*, 11423−11433.

(7) Chen, X.; Jiang, Z.; Shen, Y.; Li, R.; Fu, Y.; Liu, J.; Han, H.; Liao, H.; Cheng, X.; Jones, D. B. A.; Worden, H.; Abad, G. G. Chinese Regulations Are Working—Why Is Surface Ozone Over Industrialized Areas Still High? Applying Lessons From Northeast US Air Quality Evolution. *Geophys. Res. Lett.* **2021**, *48*, No. e2021GL092816.

(8) Yin, H.; Lu, X.; Sun, Y.; Li, K.; Gao, M.; Zheng, B.; Liu, C. Unprecedented Decline in Summertime Surface Ozone over Eastern China in 2020 Comparably Attributable to Anthropogenic Emission Reductions and Meteorology. *Environ. Res. Lett.* **2021**, *16*, 124069.

(9) Lu, X.; Hong, J.; Zhang, L.; Cooper, O. R.; Schultz, M. G.; Xu, X.; Wang, T.; Gao, M.; Zhao, Y.; Zhang, Y. Severe Surface Ozone Pollution in China: A Global Perspective. *Environ. Sci. Technol. Lett.* **2018**, *5*, 487−494.

(10) Wang, Y.; Gao, W.; Wang, S.; Song, T.; Gong, Z.; Ji, D.; Wang, L.; Liu, Z.; Tang, G.; Huo, Y.; Tian, S.; Li, J.; Li, M.; Yang, Y.; Chu, B.; Petäjä, T.; Kerminen, V.-M.; He, H.; Hao, J.; Kulmala, M.; Wang, Y.; Zhang, Y. Contrasting Trends of PM2.5 and Surface-Ozone Concentrations in China from 2013 to 2017. *Natl. Sci. Rev.* **2020**, *7*, 1331−1339.

(11) Zhang, Q.; Zheng, Y.; Tong, D.; Shao, M.; Wang, S.; Zhang, Y.; Xu, X.; Wang, J.; He, H.; Liu, W.; Ding, Y.; Lei, Y.; Li, J.; Wang, Z.; Zhang, X.; Wang, Y.; Cheng, J.; Liu, Y.; Shi, Q.; Yan, L.; Geng, G.; Hong, C.; Li, M.; Liu, F.; Zheng, B.; Cao, J.; Ding, A.; Gao, J.; Fu, Q.; Huo, J.; Liu, B.; Liu, Z.; Yang, F.; He, K.; Hao, J. Drivers of Improved PM2.5 Air Quality in China from 2013 to 2017. *Proc. Natl. Acad. Sci. U.S.A.* **2019**, *116*, 24463−24469.

(12) Zheng, B.; Tong, D.; Li, M.; Liu, F.; Hong, C.; Geng, G.; Li, H.; Li, X.; Peng, L.; Qi, J.; Yan, L.; Zhang, Y.; Zhao, H.; Zheng, Y.; He, K.; Zhang, Q. Trends in China's Anthropogenic Emissions since 2010 as the Consequence of Clean Air Actions. *Atmos. Chem. Phys.* **2018**, *18*, 14095−14111.

(13) Li, C.; Hammer, M. S.; Zheng, B.; Cohen, R. C. Accelerated Reduction of Air Pollutants in China, 2017-2020. *Sci. Total Environ.* **2022**, *803*, 150011.

(14) Shen, Y.; Jiang, F.; Feng, S.; Zheng, Y.; Cai, Z.; Lyu, X. Impact of Weather and Emission Changes on NO2 Concentrations in China during 2014−2019. *Environ. Pollut.* **2021**, *269*, 116163.

(15) Hammer, M. S.; van Donkelaar, A.; Li, C.; Lyapustin, A.; Sayer, A. M.; Hsu, N. C.; Levy, R. C.; Garay, M. J.; Kalashnikova, O. V.; Kahn, R. A.; Brauer, M.; Apte, J. S.; Henze, D. K.; Zhang, L.; Zhang,

Q.; Ford, B.; Pierce, J. R.; Martin, R. V. Global Estimates and Long-Term Trends of Fine Particulate Matter Concentrations (1998−2018). *Environ. Sci. Technol.* **2020**, *54*, 7879−7890.

(16) Liu, F.; Zhang, Q.; van der A, R. J.; Zheng, B.; Tong, D.; Yan, L.; Zheng, Y.; He, K. Recent Reduction in NO x Emissions over China: Synthesis of Satellite Observations and Emission Inventories. *Environ. Res. Lett.* **2016**, *11*, 114002.

(17) de Foy, B.; Lu, Z.; Streets, D. G. Satellite NO2 Retrievals Suggest China Has Exceeded Its NOx Reduction Goals from the Twelfth Five-Year Plan. *Sci. Rep.* **2016**, *6*, 35912.

(18) Li, K.; Jacob, D. J.; Liao, H.; Zhu, J.; Shah, V.; Shen, L.; Bates, K. H.; Zhang, Q.; Zhai, S. A Two-Pollutant Strategy for Improving Ozone and Particulate Air Quality in China. *Nat. Geosci.* **2019**, *12*, 906−910.

(19) Tan, Z.; Hofzumahaus, A.; Lu, K.; Brown, S. S.; Holland, F.; Huey, L. G.; Kiendler-Scharr, A.; Li, X.; Liu, X.; Ma, N.; Min, K.-E.; Rohrer, F.; Shao, M.; Wahner, A.; Wang, Y.; Wiedensohler, A.; Wu, Y.; Wu, Z.; Zeng, L.; Zhang, Y.; Fuchs, H. No Evidence for a Significant Impact of Heterogeneous Chemistry on Radical Concentrations in the North China Plain in Summer 2014. *Environ. Sci. Technol.* **2020**, *54*, 5973−5979.

(20) Kang, M.; Zhang, J.; Zhang, H.; Ying, Q. On the Relevancy of Observed Ozone Increase during COVID-19 Lockdown to Summertime Ozone and PM2.5 Control Policies in China. *Environ. Sci. Technol. Lett.* **2021**, *8*, 289−294.

(21) Liu, Y.; Wang, T. Worsening Urban Ozone Pollution in China from 2013 to 2017—Part 2: The Effects of Emission Changes and Implications for Multi-Pollutant Control. *Atmos. Chem. Phys.* **2020**, *20*, 6323−6337.

(22) Li, K.; Jacob, D. J.; Liao, H.; Shen, L.; Zhang, Q.; Bates, K. H. Anthropogenic Drivers of 2013−2017 Trends in Summer Surface Ozone in China. *Proc. Natl. Acad. Sci. U.S.A.* **2019**, *116*, 422−427.

(23) Wang, T.; Xue, L.; Brimblecombe, P.; Lam, Y. F.; Li, L.; Zhang, L. Ozone Pollution in China: A Review of Concentrations, Meteorological Influences, Chemical Precursors, and Effects. *Sci. Total Environ.* **2017**, *575*, 1582−1596.

(24) Li, Y.; Shi, G.; Chen, Z. Spatial and Temporal Distribution Characteristics of Ground-Level Nitrogen Dioxide and Ozone across China during 2015−2020. *Environ. Res. Lett.* **2021**, *16*, 124031.

(25) Pusede, S. E.; Cohen, R. C. On the Observed Response of Ozone to NOx and VOC Reactivity Reductions in San Joaquin Valley California 1995−Present. *Atmos. Chem. Phys.* **2012**, *12*, 8323−8339.

(26) Nussbaumer, C. M.; Cohen, R. C. The Role of Temperature and NOx in Ozone Trends in the Los Angeles Basin. *Environ. Sci. Technol.* **2020**, *54*, 15652−15659.

(27) Jin, X.; Fiore, A.; Boersma, K. F.; Smedt, I. D.; Valin, L. Inferring Changes in Summertime Surface Ozone−NOx−VOC Chemistry over U.S. Urban Areas from Two Decades of Satellite and Ground-Based Observations. *Environ. Sci. Technol.* **2020**, *54*, 6518−6529.

(28) Ivatt, P. D.; Evans, M. J.; Lewis, A. C. Suppression of Surface Ozone by an Aerosol-Inhibited Photochemical Ozone Regime. *Nat. Geosci.* **2022**, *15*, 536−540.

(29) Liu, Y.; Wang, T. Worsening Urban Ozone Pollution in China from 2013 to 2017—Part 1: The Complex and Varying Roles of Meteorology. *Atmos. Chem. Phys.* **2020**, *20*, 6305−6321.

(30) Kavassalis, S. C.; Murphy, J. G. Understanding Ozone-Meteorology Correlations: A Role for Dry Deposition. *Geophys. Res. Lett.* **2017**, *44*, 2922−2931.

(31) Ni, R.; Lin, J.; Yan, Y.; Lin, W. Foreign and Domestic Contributions to Springtime Ozone over China. *Atmos. Chem. Phys.* **2018**, *18*, 11447−11469.

(32) Lu, X.; Zhang, L.; Chen, Y.; Zhou, M.; Zheng, B.; Li, K.; Liu, Y.; Lin, J.; Fu, T. M.; Zhang, Q. Exploring 2016−2017 Surface Ozone Pollution over China: Source Contributions and Meteorological Influences. *Atmos. Chem. Phys.* **2019**, *19*, 8339−8361.

(33) Lu, X.; Ye, X.; Zhou, M.; Zhao, Y.; Weng, H.; Kong, H.; Li, K.; Gao, M.; Zheng, B.; Lin, J.; Zhou, F.; Zhang, Q.; Wu, D.; Zhang, L.; Zhang, Y. The Underappreciated Role of Agricultural Soil Nitrogen

Oxide Emissions in Ozone Pollution Regulation in North China. *Nat. Commun.* **2021**, *12*, 5021.

(34) Almaraz, M.; Bai, E.; Wang, C.; Trousdell, J.; Conley, S.; Faloona, I.; Houlton, B. Z. Agriculture Is a Major Source of NOx Pollution in California. *Sci. Adv.* **2018**, *4*, No. eaao3477.

(35) Romer, P. S.; Duffey, K. C.; Wooldridge, P. J.; Edgerton, E.; Baumann, K.; Feiner, P. A.; Miller, D. O.; Brune, W. H.; Koss, A. R.; de Gouw, J. A.; Misztal, P. K.; Goldstein, A. H.; Cohen, R. C. Effects of Temperature-Dependent NOx Emissions on Continental Ozone Production. *Atmos. Chem. Phys.* **2018**, *18*, 2601−2614.

(36) Sindelarova, K.; Granier, C.; Bouarar, I.; Guenther, A.; Tilmes, S.; Stavrakou, T.; Müller, J. F.; Kuhn, U.; Stefani, P.; Knorr, W. Global Data Set of Biogenic VOC Emissions Calculated by the MEGAN Model over the Last 30 Years. *Atmos. Chem. Phys.* **2014**, *14*, 9317−9341.

(37) Pusede, S. E.; Steiner, A. L.; Cohen, R. C. Temperature and Recent Trends in the Chemistry of Continental Surface Ozone. *Chem. Rev.* **2015**, *115*, 3898−3918.

(38) Dang, R.; Liao, H.; Fu, Y. Quantifying the Anthropogenic and Meteorological Influences on Summertime Surface Ozone in China over 2012−2017. *Sci. Total Environ.* **2021**, *754*, 142394.

(39) Wang, N.; Lyu, X.; Deng, X.; Huang, X.; Jiang, F.; Ding, A. Aggravating O3 Pollution Due to NOx Emission Control in Eastern China. *Sci. Total Environ.* **2019**, *677*, 732−744.

(40) Lou Thompson, M.; Reynolds, J.; Cox, L. H.; Guttorp, P.; Sampson, P. D. A Review of Statistical Methods for the Meteorological Adjustment of Tropospheric Ozone. *Atmos. Environ.* **2001**, *35*, 617−630.

(41) Camalier, L.; Cox, W.; Dolwick, P. The Effects of Meteorology on Ozone in Urban Areas and Their Use in Assessing Ozone Trends. *Atmos. Environ.* **2007**, *41*, 7127−7137.

(42) Grange, S. K.; Carslaw, D. C.; Lewis, A. C.; Boleti, E.; Hueglin, C. Random Forest Meteorological Normalisation Models for Swiss PM10 Trend Analysis. *Atmos. Chem. Phys.* **2018**, *18*, 6223−6239.

(43) Shi, Z.; Song, C.; Liu, B.; Lu, G.; Xu, J.; Van Vu, T. V.; Elliott, R. J. R.; Li, W.; Bloss, W. J.; Harrison, R. M. Abrupt but Smaller than Expected Changes in Surface Air Quality Attributable to COVID-19 Lockdowns. *Sci. Adv.* **2021**, *7*, No. eabd6696.

(44) Vu, T. V.; Shi, Z.; Cheng, J.; Zhang, Q.; He, K.; Wang, S.; Harrison, R. M. Assessing the Impact of Clean Air Action on Air Quality Trends in Beijing Using a Machine Learning Technique. *Atmos. Chem. Phys.* **2019**, *19*, 11303−11314.

(45) Grange, S. K.; Lee, J. D.; Drysdale, W. S.; Lewis, A. C.; Hueglin, C.; Emmenegger, L.; Carslaw, D. C. COVID-19 Lockdowns Highlight a Risk of Increasing Ozone Pollution in European Urban Areas. *Atmos. Chem. Phys.* **2021**, *21*, 4169−4185.

(46) Zhu, Q.; Laughner, J. L.; Cohen, R. C. Combining Machine Learning and Satellite Observations to Predict Spatial and Temporal Variation of near Surface OH in North American Cities. *Environ. Sci. Technol.* **2022**, *56*, 7362−7371.

(47) Zhu, Q.; Laughner, J. L.; Cohen, R. C. Estimate of OH Trends over One Decade in North American Cities. *Proc. Natl. Acad. Sci. U.S.A.* **2022**, *119*, No. e2117399119.

(48) Han, H.; Liu, J.; Shu, L.; Wang, T.; Yuan, H. Local and Synoptic Meteorological Influences on Daily Variability in Summertime Surface Ozone in Eastern China. *Atmos. Chem. Phys.* **2020**, *20*, 203−222.

(49) Simon, H.; Reff, A.; Wells, B.; Xing, J.; Frank, N. Ozone Trends Across the United States over a Period of Decreasing NOx and VOC Emissions. *Environ. Sci. Technol.* **2015**, *49*, 186−195.

(50) Chang, K.-L.; Petropavlovskikh, I.; Cooper, O. R.; Schultz, M. G.; Wang, T. Regional Trend Analysis of Surface Ozone Observations from Monitoring Networks in Eastern North America, Europe and East Asia. *Elementa* **2017**, *5*, 50.

(51) Kim, S.; McDonald, B. C.; Seo, S.; Kim, K.; Trainer, M. Understanding the Paths of Surface Ozone Abatement in the Los Angeles Basin. *J. Geophys. Res.: Atmos.* **2022**, *127*, No. e2021JD035606.

(52) Li, M.; Zhang, Q.; Zheng, B.; Tong, D.; Lei, Y.; Liu, F.; Hong, C.; Kang, S.; Yan, L.; Zhang, Y.; Bo, Y.; Su, H.; Cheng, Y.; He, K. Persistent Growth of Anthropogenic Non-Methane Volatile Organic Compound (NMVOC) Emissions in China during 1990−2017: Drivers, Speciation and Ozone Formation Potential. *Atmos. Chem. Phys.* **2019**, *19*, 8897−8913.

(53) Zimmerman, N.; Presto, A. A.; Kumar, S. P. N.; Gu, J.; Hauryliuk, A.; Robinson, E. S.; Robinson, A. L.; Subramanian, R. A Machine Learning Calibration Model Using Random Forests to Improve Sensor Performance for Lower-Cost Air Quality Monitoring. *Atmos. Meas. Tech.* **2018**, *11*, 291−313.

(54) National Development and Reform Commission of the People's Republic of China. The Fourteenth Five-Year Plan for the National Economic and Social Development of the People's Republic of China and the Outline of the Long-Term Goals for 2035. 2021, https://www.ndrc.gov.cn/xxgk/zcfb/ghwb/202103/P020210323538797779059.pdf (accessed Nov 13, 2021).

(55) Kim, J.; Shusterman, A. A.; Lieschke, K. J.; Newman, C.; Cohen, R. C. The BErkeley Atmospheric CO2 Observation Network: Field Calibration and Evaluation of Low-Cost Air Quality Sensors. *Atmos. Meas. Tech.* **2018**, *11*, 1937−1946.

(56) Laughner, J. L.; Cohen, R. C. Direct Observation of Changing NOx Lifetime in North American Cities. *Science* **2019**, *366*, 723−727.

(57) Jin, X.; Zhu, Q.; Cohen, R. C. Direct Estimates of Biomass Burning NOx Emissions and Lifetimes Using Daily Observations from TROPOMI. *Atmos. Chem. Phys.* **2021**, *21*, 15569−15587.

(58) Hui, L.; Liu, X.; Tan, Q.; Feng, M.; An, J.; Qu, Y.; Zhang, Y.; Deng, Y.; Zhai, R.; Wang, Z. VOC Characteristics, Chemical Reactivity and Sources in Urban Wuhan, Central China. *Atmos. Environ.* **2020**, *224*, 117340.

(59) Song, C.; Liu, B.; Dai, Q.; Li, H.; Mao, H. Temperature Dependence and Source Apportionment of Volatile Organic Compounds (VOCs) at an Urban Site on the North China Plain. *Atmos. Environ.* **2019**, *207*, 167−181.

(60) Jiang, X.; Li, G.; Fu, W. Government Environmental Governance, Structural Adjustment and Air Quality: A Quasi-Natural Experiment Based on the Three-Year Action Plan to Win the Blue Sky Defense War. *J. Environ. Manage.* **2021**, *277*, 111470.

(61) State Council of the People's Republic of China. Three-year Action Plan for Protecting Blue Sky. 2018, http://www.gov.cn/zhengce/content/2018-07/03/content_5303158.htm (accessed Nov 18, 2021).

(62) Zheng, B.; Zhang, Q.; Geng, G.; Chen, C.; Shi, Q.; Cui, M.; Lei, Y.; He, K. Changes in China's Anthropogenic Emissions and Air Quality during the COVID-19 Pandemic in 2020. *Earth Syst. Sci. Data* **2021**, *13*, 2895−2907.

(63) Schroeder, J. R.; Crawford, J. H.; Fried, A.; Walega, J.; Weinheimer, A.; Wisthaler, A.; Müller, M.; Mikoviny, T.; Chen, G.; Shook, M.; Blake, D. R.; Tonnesen, G. S. New Insights into the Column CH2O/NO2 Ratio as an Indicator of near-Surface Ozone Sensitivity. *J. Geophys. Res.: Atmos.* **2017**, *122*, 8885−8907.

(64) Wu, Y.; Zhang, S.; Hao, J.; Liu, H.; Wu, X.; Hu, J.; Walsh, M. P.; Wallington, T. J.; Zhang, K. M.; Stevanovic, S. On-Road Vehicle Emissions and Their Control in China: A Review and Outlook. *Sci. Total Environ.* **2017**, *574*, 332−349.

(65) Xia, S.-Y.; Wang, C.; Zhu, B.; Chen, X.; Feng, N.; Yu, G.-H.; Huang, X.-F. Long-Term Observations of Oxygenated Volatile Organic Compounds (OVOCs) in an Urban Atmosphere in Southern China, 2014−2019. *Environ. Pollut.* **2021**, *270*, 116301.

(66) Gao, W.; Tie, X.; Xu, J.; Huang, R.; Mao, X.; Zhou, G.; Chang, L. Long-Term Trend of O3 in a Mega City (Shanghai), China: Characteristics, Causes, and Interactions with Precursors. *Sci. Total Environ.* **2017**, *603−604*, 425−433.

(67) Zhang, Q.; Yuan, B.; Shao, M.; Wang, X.; Lu, S.; Lu, K.; Wang, M.; Chen, L.; Chang, C. C.; Liu, S. C. Variations of Ground-Level O3 and Its Precursors in Beijing in Summertime between 2005 and 2011. *Atmos. Chem. Phys.* **2014**, *14*, 6089−6101.

(68) The Economist. Lessons from China's rust belt. 2018, https://www.economist.com/china/2018/02/22/lessons-from-chinas-rust-belt (accessed June 29, 2022).

(69) You, H.; Yang, J.; Xue, B.; Xiao, X.; Xia, J.; Jin, C.; Li, X. Spatial Evolution of Population Change in Northeast China during 1992–2018. *Sci. Total Environ.* **2021**, *776*, 146023.

(70) Simayi, M.; Shi, Y.; Xi, Z.; Ren, J.; Hini, G.; Xie, S. Emission Trends of Industrial VOCs in China since the Clean Air Action and Future Reduction Perspectives. *Sci. Total Environ.* **2022**, *826*, 153994.

(71) Coumou, D.; Rahmstorf, S. A Decade of Weather Extremes. *Nat. Clim. Change* **2012**, *2*, 491–496.

(72) Seneviratne, S. I.; Donat, M. G.; Mueller, B.; Alexander, L. V. No Pause in the Increase of Hot Temperature Extremes. *Nat. Clim. Change* **2014**, *4*, 161–163.

📖 **Recommended by ACS**

Does Ozone Pollution Share the Same Formation Mechanisms in the Bay Areas of China?

Yangzong Zeren, Hai Guo, *et al.*

SEPTEMBER 30, 2022
ENVIRONMENTAL SCIENCE & TECHNOLOGY   READ 🔗

The Unprecedented Ozone Loss in the Arctic Winter and Spring of 2010/2011 and 2019/2020

Divakaran Ardra, Wuhu Feng, *et al.*

FEBRUARY 17, 2022
ACS EARTH AND SPACE CHEMISTRY   READ 🔗

Rapid Increases in Warm-Season Surface Ozone and Resulting Health Impact in China Since 2013

Xiao Lu, Yuanhang Zhang, *et al.*

MARCH 18, 2020
ENVIRONMENTAL SCIENCE & TECHNOLOGY LETTERS   READ 🔗

Inferring Changes in Summertime Surface Ozone–NO_x–VOC Chemistry over U.S. Urban Areas from Two Decades of Satellite and Ground-Based Observations

Xiaomeng Jin, Lukas Valin, *et al.*

APRIL 29, 2020
ENVIRONMENTAL SCIENCE & TECHNOLOGY   READ 🔗

Get More Suggestions >